water

MDPI

Article

Manganese Modified Activated Alumina through Impregnation for Enhanced Adsorption Capacity of Fluoride Ions

Yujia Gao, Kun You, Jinxiang Fu *, Juliang Wang and Weiyi Qian

School of Municipal and Environmental Engineering, Shenyang Jianzhu University, Shenyang 110168, China
* Correspondence: fujinxiang5510@163.com

Abstract: Activated alumina, with low cost to implement and consistent performance, has been widely used as a defluoridation adsorbent in contaminated groundwater. However, its application was hampered by an undesirable adsorption capacity. In the recent research, an innovative adsorbent (manganese modified activated alumina, MAA) was synthesized by impregnation method and showed a more significant adsorption capacity than that of freshly activated alumina. The scanning electron microscope, Brunauer, Emmett and Teller, X-ray diffraction spectroscopy, X-ray photoelectron spectroscopy, and Fourier transform infrared verified introduction of manganese oxides (MnOOH and MnO_2) successfully, improvement of surface microstructure and nature of single-layer adsorption, which enhanced the adsorption ability. In a short period of adsorption, the MAA maximum capacity increased from 38% to 67%. Then, batch-scale kinetic and thermodynamic adsorption investigations were performed. The high correlation coefficients R^2 (close to 1) of the quasi-second-order model, Langmuir kinetic model, and Langmuir isotherm model confirmed a better fit to the adsorption experimental data, further indicating that the diffusion of adsorbate was primarily governed by adsorption onto the active sites and the adsorption of fluoride on MAA was single-layer physical adsorption. This paper provides an approach to modifying activated alumina as a groundwater fluoride adsorbent.

Keywords: defluoridation; manganese modified activated alumina (MAA); adsorption; kinetic study

Citation: Gao, Y.; You, K.; Fu, J.; Wang, J.; Qian, W. Manganese Modified Activated Alumina through Impregnation for Enhanced Adsorption Capacity of Fluoride Ions. *Water* **2022**, *14*, 2673. https://doi.org/10.3390/w14172673

Academic Editor: Yongchang Sun

Received: 28 July 2022
Accepted: 22 August 2022
Published: 29 August 2022

1. Introduction

Fluoride, generated from geochemical and anthropological activities is widely distributed throughout the world, posing increasing threats to water security [1]. Long-term intake of fluoride ions will have a diverse impact on human health depending on their amount and concentration. The formation and maintenance of bones and teeth during childhood will be curtailed by the low concentration of fluoride water (0.5 mg/L) [2,3]. Whereas exposure to a high-fluoride medium might pose a concern to human health, such as fluorosis [4,5]. The World Health Organization (WHO) established a limit of 1.5 mg/L for fluoride-containing water in an effort to raise awareness of fluoride pollution [6]. China, one of the most affected nations, has extensively distributed high fluoride groundwater (up to 15.36 mg/L), as Luo pointed out, making it imperative to develop defluoridation techniques [7,8].

Traditional treatment technologies such as ion exchange [9,10], precipitation, electrodialysis [11], membrane filtration [12], and adsorption [13] have been applied in the defluoridation process. Nevertheless, the aforementioned technologies have inherent drawbacks, such as high implementation cost, high pH dependence, the possibility of secondary contamination, and the presence of a substantial volume of residual sludge. Although equipment for defluoridation has been delivered and technologies for enhanced

removal efficiency have been developed, ensuring the safety of drinking water is an ongoing challenge in the present day.

Comparatively, assumed as an environmental-friendly and sustainable technology, adsorption has gotten considerable attention on account of its high efficiency, low cost of adsorbents, unsurpassed simplicity and no additional chemicals and energy requirements [14,15]. The common-used adsorbents are chitosan, zeolite, polymeric materials, and activated alumina (AA) [16,17]. Although they have the capacity to diminish fluoride concentration in aquatic water, few satisfactory results were received [18]. AA claimed as a mainstream adsorbent has been utilized in groundwater treatment. Recently, modification of porous AA, as a new approach for fluoride removal use has been explored by scholars [19]. By increasing the surface area, the functional group content, and the pore structure through impregnation, the adsorption capability of AA might be boosted. Manganese dioxide (MnO_2) exhibited a specific large surface area, which can provide the reaction with additional active sites [20]. Moreover, as a result of the great hydrophilicity of manganese hydroxide (MnOOH), the hydroxyl oxide surface in an aqueous solution becomes highly hydroxylated and hydrophilic. Among the three isomers (α-MnOOH, β-MnOOH, γ-MnOOH), γ-MnOOH is the most stable and shows its excellent adsorption performance [21]. Herein, manganese modified AA was selected upon the characteristics mentioned above for fluoride removal [22].

Based on this, a promising adsorbent fabricated by manganese oxides impregnating had been applied in high fluoride medium, aiming to establish effective and stable defluoridation ability. Integration with an analytical characterization of adsorbent, the variations of element composition, functional group, and microstructure of MAA were clarified. Furthermore, the obtained sample was subjected to adsorption kinetic and thermodynamic experiments and fitted by the quasi-first-order model, quasi-second-order model, film diffusion model, Boyd model, Langmuir kinetics model, Langmuir isotherm model, and Freundlich model, respectively. A mechanistic description was also investigated to understand the contribution of manganese oxides in the system.

2. Materials and Methods

2.1. Materials

Freshly activated alumina of 1–2 nm, sodium fluoride (NaF), ammonium ferrous sulfate ($(NH_4)_2Fe(SO_4)_2{\cdot}6H_2O$), Manganese chloride ($MnCl_2$), hydroxylamine hydrochloride (H_4ClNO), ammonia ($NH_3{\cdot}H_2O$) were purchased from Sinopharm Chemical Reagent Co., Ltd. (Beijing, China). Reagents (aluminum sulfate ($Al_2(SO_4)_3$), manganese sulfate ($MnSO_4$), hydrochloric acid (HCl), phenanthroline ($C_{12}H_8N_2$), ammonium acetate (CH_3COONH_4), glacial acetic acid (CH_3COOH) were supplied by Tianjin Kemiou Chemical Reagent Co., Ltd. (Tianjin, China). Purchased from Tianjin Damao Chemical Reagent Factory (Tianjin, China) and America HACH company (Ames, IA, USA), Hydrogen peroxide (H_2O_2) and SPADNS reagent were used in this study. Chemicals were all used as received and dissolved in deionized water (resistivity of 18.20 MΩ·cm) to prepare experimental solutions.

2.2. Preparation of the Adsorbent

As Figure S1 showed, MAA was synthesized by the impregnation method. 30 g of fresh AA particles (1–2 mm in diameter) were added into a beaker with 150 mL 0.05 mol/L $MnSO_4$ solution. The reaction lasted for 6 h in a magnetically coupled electric stirrer which was set to heat up to 388 K at the speed of 145 r/min. Under continuous stirring, 5.1 mL of 30% H_2O_2 were dipped into the system to generate manganese oxides. At this time, the insoluble white cloudy manganese hydroxide was produced. Then, 75 mL of 25% $NH_3{\cdot}H_2O$ was added to the mixture to produce a strong acid ammonium salt capable of dissolving manganese hydroxide. Clearly, brown sediments were produced during this synthetic process. The resultant MAA was dried and collected in the oven for 2 h at 373 K

and flushed with deionized water every 8 times. Ultimately, the resulting materials were dried at 373 K for four hours before being cooled to room temperature. The adsorbent, dubbed MAA, was prepared for further use.

2.3. Characterizations of the adsorbent

Conforming to the Standard Test Method for Drinking Water (GB/T 57750-2006), the concentration of fluoride was 1 mg/L. The concentration of fluoride ions and temperature were detected and analyzed by fluorometric spectrophotometry and direct-reading method, respectively. A scanning electron microscope (SEM, Hitachi, S-4800, Tokyo, Japan) was used to observe the changes in the surface microstructure of the particles. The photomicrographs for each were recorded under the accelerating voltage of 5 kV and constant temperature. Measured by Brunner Emmet Teller (BET, Autosorb-IQ2-MP, Quantachrome, Boynton Beach, FL, USA), the pore parameters and surface area were computed. The pore parameters were calculated using equation (P/P_0 = 0.005–0.3), the total pore volume was measured at P/P_0 = 0.99 and the average pore diameter was computed by 4 V_t/S_t. The frame structure and chemical compositions were detected by X-ray diffraction spectroscopy (XRD, Spectris, Amsterdam, the Netherlands), which under the condition of tube voltage 40 kV, tube current 40 mA, radiation source Cu target, K^a ray, γ= 0.15406 nm, scanning range 5–90° and scanning speed 5°/min. The binding energy of the samples was analyzed to evaluate the composition of the manganese element by X-ray photoelectron spectroscopy (XPS, Thermo Fisher Scientific Co., ESCALAB 250Xi, Shanghai, China), and the spectra calibrated to the Mn 2p peak at 641.5 eV and 653.8 eV. A Fourier Transform Infrared (FT-IR, Thermo Nicolet Corporation, NICOLET iS50, Waltham, MA, USA) spectroscopy of particles was used at 400–4000 cm^{-1}, and each was scanned 32 times to analyze infrared adsorption spectroscopy in transmission mode.

2.4. Adsorption Studies

This test employed the configuration of simulated water samples. Initially, 0.2210 g of NaF dried at 378–383 K for 2 h, 0.7020 g of $(NH_4)_2Fe(SO_4)_2{\cdot}6H_2O$ and 0.2290 g of $MnCl_2$ were dissolved in a specific volume of distilled water and fixed to 1000 mL, with the concentration of each standard solution being 100 mg/L. To simulate real groundwater with high fluoride, iron and manganese, 200 mL beakers holding 100 mL of simulated laboratory solution with a specific quantity of standard solution were made. Then, the solution was mixed with a certain amount of MAA for a predetermined contact time. Experiments on a batch scale were conducted in an incubator at 120 rpm and a constant temperature. The pH value was adjusted with 1 mol/L HCl or 1 mol/L NaOH in advance. To ensure the reproducibility of the data, three parallel experiments were undertaken, and error bars were also included in the image.

2.4.1. Adsorption Kinetics

Experiments on a batch scale were conducted in 200 mL beakers holding 100 mL of simulated laboratory solution in an incubator at 120 rpm and a constant temperature. The pH value was adjusted with 1 mol/L HCl or 1 mol/L NaOH in advance. To simulate real groundwater with high fluoride, iron and manganese, the reaction solution was mixed with a certain amount of MAA for a predetermined contact time. To ensure the reproducibility of the data, three parallel experiments were undertaken, and error bars were also included in the image. External mass transfer, internal mass transfer, and adsorption on active sides, all consist of the adsorbate transfer processes [23]. This study employed two kinetic classical models and three diffusion models, including the quasi-first-order model [24], quasi-second-order model [25], film diffusion model [26], Boyd model [27] and Langmuir kinetics model [28], to further discuss the rate-limiting procedure and the key kinetic adsorption mass transfer step. The fluoride ions

concentration was detected at certain time intervals and the adsorption quantity (q_t mg/g) representing adsorption ability was calculated as the following equation:

$$q_t = (C_0 - C_t)V/w \quad (1)$$

where C_t (mg/L) and w (g) represent the concentration of fluoride ions at time t (min) and the weight of the adsorbent. The mathematical expressions can be written as follows:

Quasi-first-order model:

$$\ln(q_e - q_t) = \ln(q_e) - K_1 t \quad (2)$$

Quasi-second-order model:

$$t/q_t = 1/K_2 q_e^2 + t/q_e \quad (3)$$

Film diffusion model:

$$\ln(1 - q_t/q_e) = -K_3 t + A \quad (4)$$

Boyd model:

$$F = q_t/q_e = 1 - 6/n^2 \sum_{n=1}^{\infty} 1/n^2 \exp(-n^2 Bt) \quad (5)$$

Langmuir kinetics model:

$$dq_t/dt = K_a C_t(q_e - q_t) - K_d q_t \quad (6)$$

where q_t and q_e (mg/g) are the amounts of fluoride adsorbed at time t and equilibrium, respectively. K_1 (1/min) and K_2 (g/mg·min) are the rates constant of the quasi-first-order equation and quasi-second-order equation. K_3 (1/min) and A are the liquid film diffusion constants. F is the fractional achievement of equilibrium, and time t and B_t are mathematical functions of F. As for K_a (L/mg·h) and K_d (h^{-1}) are the adsorption and desorption rate constants, respectively.

2.4.2. Thermodynamic Study

The conventional Langmuir and Freundlich isotherm models were mentioned and evaluated in order to discuss the effect of temperature on MAA. The mathematical expressions are displayed in accordance with the following formula:

Langmuir isotherm model:

$$q_e = K_L q_{max} C_e/(1 + K_L C_e) \quad (7)$$

Freundlich isotherm model:

$$\ln(q_e) = \ln(K_F) + \ln(C_e)/n \quad (8)$$

where q_D (mg/g) is the maximum fluoride adsorbed, Ce is the concentration of adsorbent at equilibrium and K_L (J/mol) is the constant of the Langmuir isotherm model.

The thermodynamic parameters, Gibbs free energy change (ΔGo), enthalpy change (ΔHo), and entropy change (ΔSo) were calculated to expound the interaction of MAA and fluoride ions. The mathematical expressions were detailed as follows:

$$\Delta G = -RT\ln K_d \quad (9)$$

$$\ln K = \Delta S/R - \Delta H/RT \quad (10)$$

$$\ln(1/C_e) = -\Delta H/RT + \ln K_0 \quad (11)$$

where K_d obtained from the Langmuir model, represents the adsorption equilibrium constant. R is the universal Gas constant value of 8.314 J/(mol·K), and T is the temperature

(K). The available values of ΔH and ΔS severed as the slope and intercept from a linear plot between $\ln_k$ versus 1/T.

2.4.3. Effect of Coexisting Ions

The common-existed anions (e.g., chloride, carbonate, bicarbonate, phosphate, and nitrate) that could be in groundwater, may affect the fluoride removal effectiveness. Due to their electronegative nature, the adsorption of fluoride may be impeded by the anions indicated. Determining the interference effect of these co-existing ions is therefore critical. The prepared concentration of ions with sodium salts ranged from 0 to 300 mg/L, respectively.

3. Results and Discussion

3.1. Characterization of the Adsorbent

To explore the morphology changes of the adsorbent during the modification process (as Figure S1 showed), SEM images of AA and MAA were captured. Significantly, as depicted in Figure 1a, accumulated impurities and bulks heaped up in the present structure of fresh AA led to the immature pore structure. Compared to Figure 1b, the surface of the changed particles exhibited significant alterations. Partial impurities were removed that changed the rough surface of AA. In the meantime, a certain number of pore channels uniformed and broadened, which may result in an increased defluoridation potential [29]. Especially, convex spinous structure occurred which further demonstrated the successful introduction of manganese oxides.

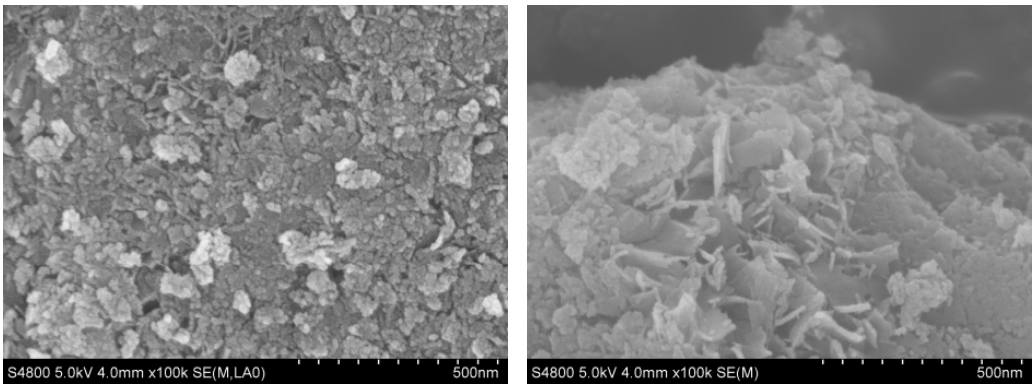

(**a**) (**b**)

Figure 1. SEM image of fresh alumina (**a**), MAA (**b**).

BET tests were also conducted to manifest the pore parameters of the adsorbent. The possessed pore diameter and surface area of nascent AA were approximately 0.434 nm and 287.259 m^2/g, respectively (Table S1). After the impregnation process, the pore size was slightly diminished to 0.377 nm with certain manganese oxides clogged, while the average surface area was elevated to 295.599 m^2/g. The enlarged specific surface area facilitated the exposure of adsorption sites and benefited from fluoride removal. As described in Figure 2, the plots of N_2 adsorption-desorption isotherm with parallel trends were discussed. According to the standard of IUPAC, the nature of the isotherm curve for both the samples were belong to type IV with an H3 hysteresis loop. Implied that the particle size of the adsorbent was irregular [30]. These detected results confirmed that the impregnation process induces minute alterations in frame structure.

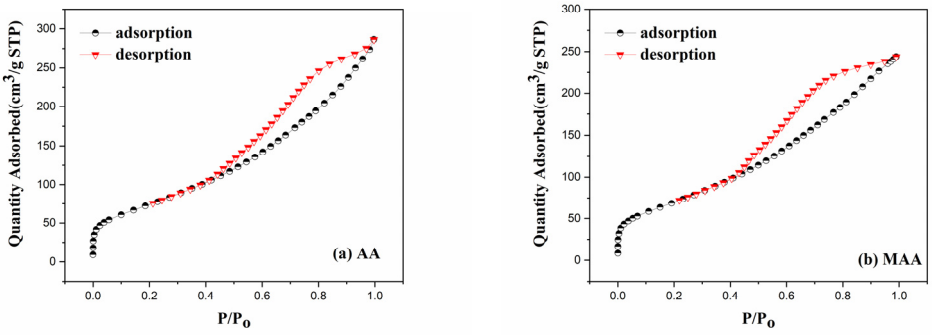

(**a**) (**b**)

Figure 2. N_2 adsorption-desorption isotherm plot of fresh AA (**a**) and MAA (**b**) from BET analysis.

The results of frame structure and elemental composition upon XRD analysis of fresh AA, and MAA were given in Figure 3a. As compared through the spectra, the crystal structure of the adsorbents was similar, barely with any changes on it. The sharp diffraction peaks were detected by the emerged (2 2 0), (3 1 1), (2 2 2), (4 0 0) (Al_2O_3) for both adsorbents were compatible with current literature values JCPDS No.29-0063. Furtherly, new characteristic peaks at (1 0 1), (2 1 1), (1 4 1) (JCPDS No.74-1842) and (1 1 0), (1 0 1), (2 2 0), (3 1 1) (JCPDS No.72-1984), corresponding to γ-MnOOH and MnO_2, respectively. It revealed that the major oxides of fresh AA were Al_2O_3 and manganese compounds successfully loaded on the surface of the modified samples following impregnation.

Using XPS analysis, the chemical composition of the modified particles was further investigated. As shown in Figure 3b, Al 1s, C 1s, O 1s, along with Mn 2p were detected in survey scan spectra with peaks located at 80 eV, 293 eV, 537 eV, and 660 eV, respectively. As pointed out in Figure 3b, the binding energies of Mn 2p in MAA were mainly peaked at 641.5 eV and 653.8 eV, respectively, which assigned to MnOOH and MnO_2. The presence of two divided bands indicated the loading of manganese species, and the coexistence of MnOOH and MnO_2 was the primary factor that facilitated the adsorption procedure. Meanwhile, the content of MnOOH and MnO_2 were accounting for 48.67 and 51.33%, which further validated the XRD analysis results.

The FT–IR spectrum of the adsorbent was illustrated in Figure 3c to explore the changes in chemical groups during the adsorption procedure. Peaks at 3450 cm^{-1}, 1630 cm^{-1}, and 542 cm^{-1} were found and further verified as characteristic peaks for −OH stretching vibration, water molecules bending vibration, and the combination of Al-O and Mn-O bonds, respectively. Especially, the intensified peak at 3450 cm^{-1} of fluoride adsorbed AA was ascribed to introducing manganese oxide, which increases the content of hydroxyl groups. Moreover, in spectra of depleted MAA, the intensity of water molecules bending vibration increased distinctly at the peak of 1630 cm^{-1}. This consequence proves that hydroxyl compounds have been substituted which was considered to be ion exchange interaction. Located at 542 cm^{-1}, was identical to the combined stretching vibrations of Al-O and Mn-O. A step further, no significant variations of peak location appeared in the adsorption process, suggesting that no other chemical groups were generated and presumably be electrostatic adsorption.

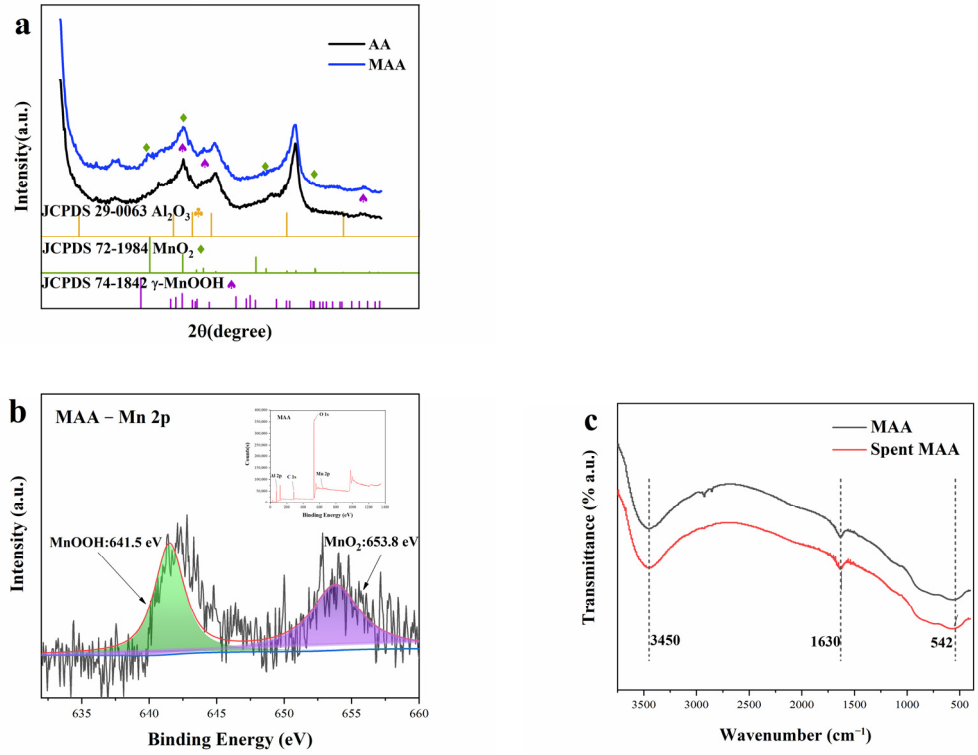

Figure 3. XRD analysis of fresh alumina and MAA (**a**); XPS spectra of Mn 2p for MAA (**b**); FT-IR spectrum of fresh alumina and MAA (**c**).

3.2. Comparison of Fresh Adsorbent with MAA

Compared to fresh AA that was washed with deionized water, the adsorption capacity of impregnated MAA for fluoride ions was astronomically higher. As demonstrated in Figure 4, the MAA particles exhibited a distinct increase in adsorption capacity by 29% as compared to the control. On the basis of SEM and BET, the improvement of the structure of pore nature and increased specific surface area both took effects the adsorption process.

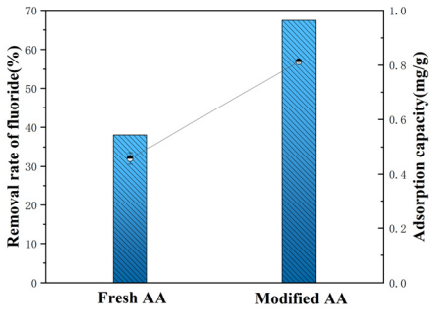

Figure 4. Comparison of fluoride removal effect on fresh AA and MAA.

Reaction conditions: $[\text{Fluoride concentration}]_0$ = 8.5 mg/L, [Adsorbent dosage] = 7 g/L, [Reaction time] = 2 h, pH_0 = 4.2 and T = 298 K.

3.3. Effect of Parameters on Fluoride Removal

3.3.1. Effect of Competing for Co-Existing Anions on MAA

To simulate real groundwater, the adsorption selectivity of MAA towards fluoride ions was investigated in the presence of ubiquitous anions. Different anionic strengths from 0 to 300 mg/L were employed in the experiment. As demonstrated in Figure 5a, the removal efficiency of fluoride all declined to varying degrees compared to the absence of anions in the system. Among them, phosphate had the strongest hindrance to fluoride adsorption performance whereas chloride, carbonate, and nitrate showed a slight decrease in fluoride efficiency of MAA. When phosphate ions upgraded from 0 to 300 mg/L, the percent fluoride removal decreased sharply from 73.81 to 17.37%. On one hand, excessive PO_4^{3-} exhibited stronger affinity with adsorption active sites on the surface of MAA and would cause adsorption competition with F^-, for another hand, higher negative charge density of trivalent anion may decrease the number of adsorption sites. The adverse effect of competing anions on defluoridation, by and large, was in the sequence of $PO_4^{3-} > CO_3^{2-} > HCO_3^- > Cl^- > NO_3^-$.

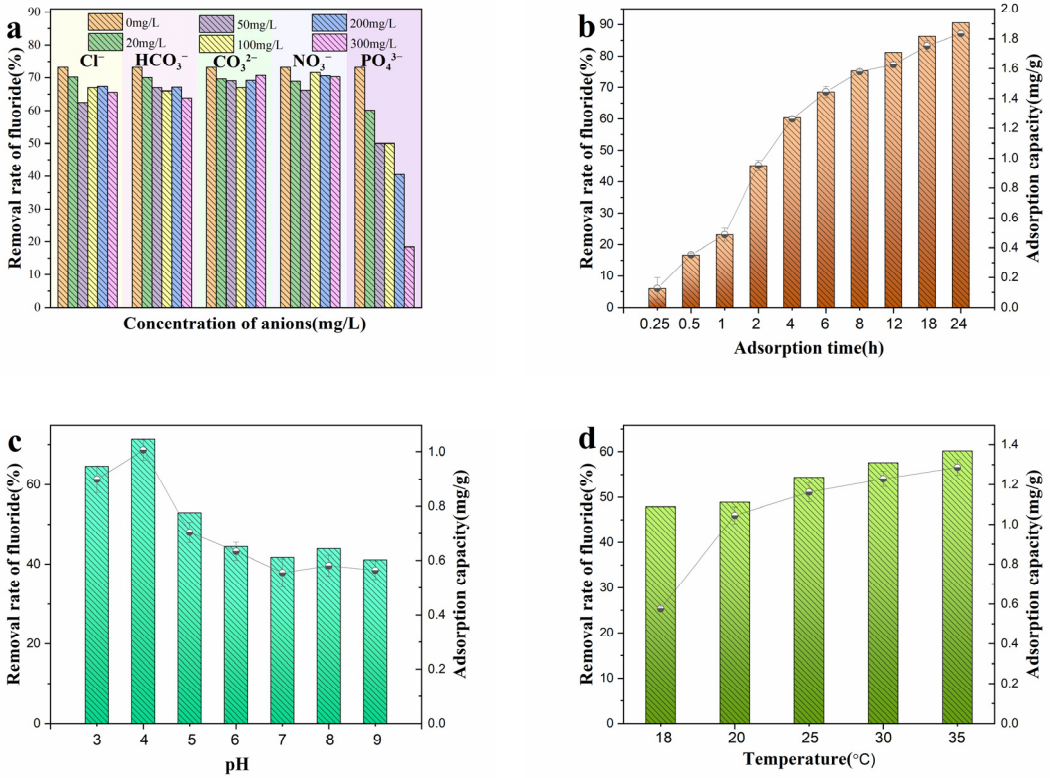

Figure 5. Effect of parameters on removal effect of MAA: competing for co-existing anions (**a**), temperature (**b**), initial pH (**c**), reaction time (**d**).

3.3.2. Effect of Contacting Time on MAA

Figure 5b illustrated the effect of reaction time on fluoride removal by the modified particles. As anticipated, the amount of fluoride adsorbed enhanced with further increment in the contacting time. This could be explained by the unsaturated adsorbent reaching equilibrium of adsorption. Comparatively, in the initial stage, the slope had the highest value, and further increase of time to 8 h would lead to a distinct drop, with the slope reaching its lowest point at 12 h. The mentioned results may be largely attributable to the diffusion route of the adsorbate enormously, which began with the external diffusion pro-

cess, continued with the internal diffusion process, and concluded with the active site adsorption phase. The observed phenomenon of manganese oxide leaching in a solution of strong acid cannot be disregarded. It has been noticed that manganese oxides began to leach below pH 4 when a long contacting time was chosen (>24 h) and can be summarized as the reaction of MnOOH with hydrogen ions, as shown in Equation (12) [31].

$$2MnOOH + 2H^+ = Mn^{2+} + MnO_2 + 2H_2O \quad (12)$$

3.3.3. Effect of Temperature on MAA

As one of the most essential adsorption parameter factors, temperature was chosen for relevant experiments. Provided in Figure 5c, was the effect of temperature on MAA. In the selected range of 298–318 K, the removal efficiency increased steadily, which was mainly due to the heat-adsorption reaction on MAA.

3.3.4. Effect of Initial pH on MAA

Regarded as the significant factor driving the removal efficiency of fluoride, the relevant experiment was performed. Chen indicated that in a strong acid medium (pH was set below 2) HF will generate a to obstacle the adsorption process [6]. Herein, in this work, different pH values ranging from 3 to 10 were set. As displayed in Figure 5d, the adsorption process was extremely highly pH-dependent and the preferable removal effect, i.e., 59.18%, was reached after 2 h of reaction at a pH of 4. Meanwhile, the modified AA exhibited a wide effective pH range, with maximum percent removal varying from 29.02% to 59.18%. The wide range of applicable pH indicated that MAA could be effectively severed as a novel adsorbent for the removal of fluoride from polluted groundwater. Ranged from 3–4 of pH value, adsorption capacity manifested an obvious rise. According to Bingcai Pan [32], on the one hand, free fluoride ions were insufficient to exchange with Hydroxide ions at lower pH, on another hand, a 10-fold concentration of chloride ions would induce a stronger anion competition effect with fluoride. Apparently, on increased pH value from 5 to 9, the adsorption capacity of fluoride decreased steadily. This could be attributed to the competition of excess OH^- ions and negatively charged fluoride ions, which weakened the interaction of electrostatic forces. Considering the manganese leaching under acidic conditions, the performance of adsorption at pH 5 was investigated further.

3.4. Kinetic Modeling

Under different circumstances, the adsorption kinetics specified the rate of retention or released of the adsorbate from the aqueous solution to the solid phase interface [33]. Using batch experiments, the adsorption mass transfer kinetic, which was governed by external diffusion, internal diffusion, and adsorption on active sides, was investigated. Corresponding to the typical concentration of high-fluoridated groundwater, 3, 6, and 12 mg/L of contaminant polluted were selected for further kinetic discussion. As depicted in Figure 6a, a comparison of adsorption dynamic data revealed a similar upward trend. The adsorption process on MAA was time-limited, as the rate of fluoride adsorption reached its maximum value at an early stage and then gradually decreased until it reached solid-liquid equilibrium as time progressed. Especially, the adsorption capacity increased rapidly in the initial stage (0–600 min) which was mainly governed by external diffusion. Subsequently, from 600 min to 1500 min, the adsorption rate slowed down. This could be attributed to the fact that MAA was gradually covered by fluoride ions, particularly at active sites and pores, a phenomenon referred to as internal diffusion of the adsorbate. Then, in the final age, a low velocity was confirmed owing to the progressive occupation of a specific number of active sites. The adsorption reaction tended to be stable, that is to say, the adsorption came to an equilibrium state.

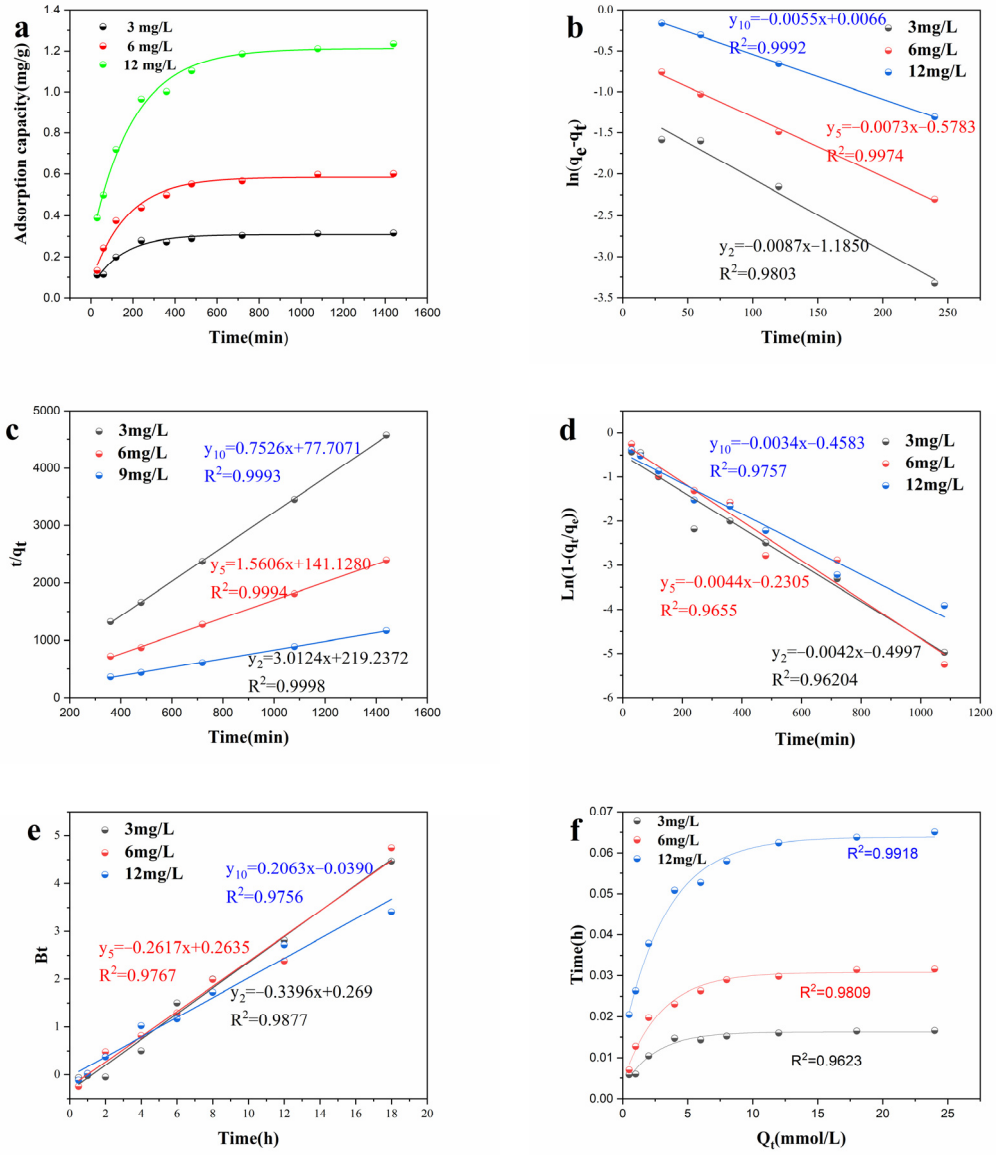

Figure 6. Adsorption kinetic curve on MAA (**a**); adsorption kinetic experimental data at 3 mg/L, 6 mg/L, and 12 mg/L of initial fluoride concentration Kinetic model of quasi-first-order (**b**), quasi-second-order (**c**), film diffusion (**d**), Boyd diffusion (**e**), Langmuir kinetics (**f**) fitting on MAA.

3.4.1. Quasi-First-Order Model and Quasi-Second Model

The quasi-first-order kinetic model was established to evaluate the adsorption reaction. In addition, Guo pointed out that the requirements for the quasi-first-order model were: (1) high initial concentration of the adsorbate; (2) application of the initial adsorption stage; and (3) the presence of a small number of active sites on the adsorbent [23]. Thus, as represented in Figure 6b, the experimental data of the kinetic study were fitted by the quasi-first-order model (Equation (2)) from 0 to 540 min. The regression coefficients R^2 corresponding to 6 and 12 mg/L of fluoride initial concentration were 0.9974 and 0.9992 as evaluated. As summarized in Table S2, parameters q_e and K_1 were calculated by plotting $\ln(q_e-q_t)$ versus t. To a step further, the values of K_1 were used to describe the ratio of fluoride removal. The calculated parameters expounded that during the adsorption process, some fluoride ions passed through the orifice and diffused into the pores of MAA.

The quasi-second-order adsorption rate of modified AA was calculated based on Equation (3) and the results were manifested in Figure 6c. As Guo suggested, the quasi-

second-order model should be fitted under conditions of low initial concentration of the adsorbate, the abundance of active sites, and the final stage of adsorption [23]. Additionally, Mahmoud et al. pointed that there was a significant relationship between quasi-second order in adsorption capacity and effective active sites [34]. Figure 6c demonstrated that the quasi-second-order model could perfectly describe the entire defluoridation process, which was consistent with the previous studies [35]. The parameters of the quasi-second-order model were presented in Table S2. It is worth noting that high R^2 values based on 3, 6, and 12 mg/L of initial fluoride were 0.9993, 0.9994, and 0.9998, respectively, which were higher than that of the quasi-first-order model. Additionally, the expressed parameter of K_2 was calculated. In comparison with K_1, the higher K_2 indicated that the adsorption on MAA followed second-order kinetics better. Therefore, the modified AA had a large number of active sides and some fluoride ions adsorbed owing to the fluoride-hydroxyl exchange reaction.

3.4.2. External Mass Transfer Process

The external diffusion process of MAA on fluoride adsorption was examined by kinetic experiments. This behavior referred to the diffusion of adsorbate from solution to the liquid film surrounding the adsorbent to reach the external surface of the MAA particles, corresponding to the highest slope in the initial stage of Figure 6a. Ahmed verified that the main step limiting the rate of adsorption was external diffusion when the linear curve of $\ln(1 - q_t/q_e)$ versus t passed through the origin [26]. Thus, the film diffusion model (Equation (4)) was fitted, and the plot was depicted in Figure 6d. Meanwhile, the calculated parameters R^2, A, and K_3 were listed in Table S2. Noted that all the fitting curves did not pass through the original point and R^2 were 0.9620, 0.9655, and 0.9757, respectively. The above results revealed that the selective-limiting step was not the external diffusion and there existed other transport pathways controlling the adsorption performance to reach equilibrium.

3.4.3. Internal Mass Transfer Resistance

Boyd developed a rate equation based on the assumption that the diffusion of adsorbate within the adsorbent controls the rate [27]. To determine the effect of intraparticle diffusion of adsorbate, the Boyd model was used to fit the kinetic data (Figure 6e). The linear form of Equation (5) could be simplified as:

$$B_t = -0.4977 - \ln(1 - F) \quad (13)$$

Then, the curve of B_t versus t was plotted for each q_t value. If this plot is a straight line and goes through (0, 0), the internal mass transfer will be the primary rate-controlling step. Nevertheless, the curve avoided the point of origin and the R^2 values were 0.9877, 0.9767, and 0.9756, respectively. Thus, it is reasonable to conclude that the overall rate is not only affected by internal diffusion.

3.4.4. Adsorption onto the Active Sites

The Langmuir kinetics model was adopted to investigate the step of adsorption on active sites, as described in Figure 6f. The model assumes that the diffusion is negligible, and the slowest step of adsorption is onto active sites. As shown in Table S2, parameters R^2 (0.9623, 0.9809 and 0.9918) were estimated. Values of determination coefficient R^2 were higher than either film the diffusion model or Boyd model, suggesting that the Langmuir kinetics model gave a better fit. The preceding studies demonstrated that adsorption onto active surfaces played the dominant role.

3.5. Isotherm Modeling

To explore the mechanism of temperature on the defluoridation of MAA, the isotherm behavior of MAA was fitted by Langmuir and Freundlich isotherm models, which was helpful to further investigate the effect of adsorption, nature of adsorbent, and the behavior of fluoride removal. Figure 7 showed the higher R^2 values of the Langmuir model indicated that the adsorption isotherm was more of a Langmuir fit rather than Freundlich. In addition, Mahmoud pointed that the Langmuir adsorption isotherm was proportional to the number of active sites on the adsorbent throughout the adsorption process [33]. The above result further verified that the removal of fluoride ions was mainly the result of single-layer adsorption, active sites played the dominating role in the whole process and the theoretical maximum adsorption capacity reached 1.97 mg/g.

The obtained thermodynamic qualities were examined to further discuss the mechanism of adsorptions using Gibbs free energy change (ΔG), enthalpy (ΔS), and entropy (ΔH). Given in Table S3 were the values of the parameters mentioned above. The negative ΔG assumed the adsorption process was spontaneous. To a step further, the positive values of ΔS and ΔH for fluoride adsorption indicated the endothermic behavior, which, along with the enhanced randomness at the solid-liquid interface, suggested that the higher temperature favored the degree of adsorption and that the spontaneity was owing to the increase in entropy.

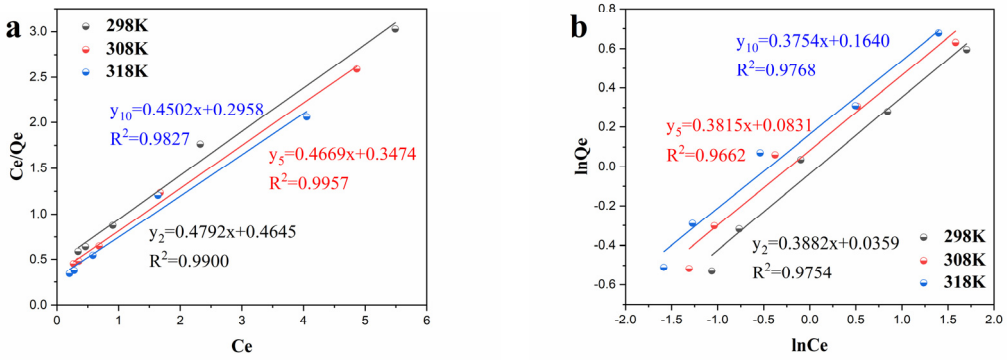

Figure 7. Curve of Langmuir (**a**) and Freundlich (**b**) isotherm fitting for fluoride adsorption on MAA.

3.6. Effect of MAA on Fluoride Removal

The observed adsorption preference of MAA toward fluoride ions can be extrapolated based on characteristic features. Briefly, the adsorption process may be the reason for electrostatic attraction and ion exchange. When in the acidic medium, MAA inevitably absorbed water molecules which occurred surface hydroxylation and lead to the surface of MAA electropositive [14]. Then, the surface hydroxyl group was protonated based on XRD and FT-IR. Concurrently, the released hydroxyl caused the pH to rise. Simultaneously, MnOOH was reduced to $Mn(OH)_2$. Due to the comparable ionic radius of the hydrate, fluoride is swapped with hydroxyl groups. In the adsorption process, by and large, one is the negatively charged fluoride bound to the positive surface by electrostatic force (Equation (14)), and the other is fluoride ion exchanged with hydroxyl groups due to the similar hydrated ionic radius (Equations (15) and (16)).

$$AlOH + H_2O - H^+ + F^- = AlOH - H^+F^- + H_2O \quad (14)$$

$$(Al_2O_3)_nMnOOH + H_2O \rightarrow (Al_2O_3)_nMn(OH)_2OH \quad (15)$$

$$R(Al_2O_3)_nMn(OH)_2 + 2F^- \rightarrow R(Al_2O_3)_nMnF_2 + 2OH^- \quad (16)$$

3.7. Comparison to Literature

In a comparison of various adsorbents used for the removal of fluoride ions, it was found that: (1) MAA has a relatively high adsorption capacity and a short adsorption equilibrium period. The maximum Langmuir calculated adsorption capacity of MAA (1.81 mg/g) prepared in this work was found to be higher than that of our previously fabricated [35] (1.45 mg/g) with 12 h of shorter contact time to reach equilibrium state under conditions of 298 K; (2) MAA performed well throughout a wide pH range, with the maximum removal rate decreasing by just 30% when the pH was adjusted from 3 to 9. In contrast, when the pH was changed from 6.7 to 9, the efficacy of fluoride removal from lanthanum-impregnated chitosan [36] dropped by about 75%. Additionally, the fluoride removal rate rapidly decreased when the pH of sawdust impregnated ferric hydroxide and activated alumina (SFAA) was increased above 7 [37]. (3) Additionally, manganese modified activated alumina was cost-effective in fluoride treatment. The following was a breakdown of the cost effectiveness of several fluoride removal adsorbents.

Cost of per kg of activated alumina = 0.59–1.33 USD/kg
Cost of per kg of chitosan = 13.35–14.83 USD/kg
Cost of per kg of coconut shell activated carbon = 1.26–1.63 USD/kg
Cost of per kg of red mud = 2.22–2.67 USD/kg

Consequently, it was plausible to believe that MAA was a promising fluoride removal adsorbent.

3.8. The Performance of MAA in Real Water

Despite the fact that activated alumina may efficiently lower the concentration of fluoride ions in drinking water, there are still several restrictions on the practical implementation of this technology, such as an unstable fluoride removal effect. Therefore, in this experiment, manganese-modified activated alumina was applied to fluoride-rich groundwater in order to evaluate its efficacy as a treatment agent. As shown in Figure 8, the fluoride removal rate of MAA could fast reach 53.51% after 2 h of contact, but AA's fluoride removal rate was only 20.18% at the same time. After 8 h, the fluoride removal rate of MAA could reach 70.18% nearly twice that of AA. From the test results, it can be shown that both the adsorption rate and adsorption quantity increased significantly following the impregnation.

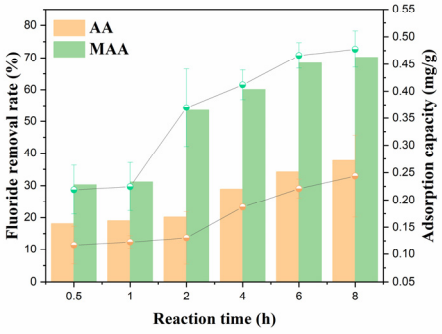

Figure 8. Comparison of fluoride removal effect on fresh AA and MAA in real contaminated water.

Reaction conditions: [Fluoride concentration]$_0$ = 4.5 mg/L, [Adsorbent dosage] = 7 g/L, pH_0 = 4.18 and T = 298 K.

4. Conclusions

This paper has shown that manganese impregnation provided a novel approach to fabricating the modified adsorbent, and the findings demonstrated that MAA possessed

a remarkable accelerated adsorption capacity, resulting in a nearly 30% increase in fluoride removal efficiency compared to the control. The adsorption kinetics was convinced to follow the quasi-second-order model that assumed the adsorption process as physical. The defluoridation kinetics on MAA was better described by the quasi-second-order and Langmuir kinetics model, which illustrated that the adsorption on active sides played a crucial part. Langmuir isotherm model gave a better fit of thermodynamics data and the theoretical maximum adsorption capacity reached 1.97 mg/g. The preceding data suggested that the adsorption process was spontaneous and endothermic. According to XRD, the increased fluoride adsorption capability was attributable to the incorporation of MnO_2 and γ-MnOOH onto the surface of AA. Electrostatic attraction and ion exchange effect were deduced to contribute to the fluoride removal accordingly. Overall, MAA is a promising tool for fluoride removal and was a promising adsorbent that can offer a reference for groundwater treatment.

Supplementary Materials: The following are available online at https://www.mdpi.com/article/10.3390/w14172673/s1, Figure S1: The diagram of impregnation equipment, Table S1: Parameters of pore structure of AA and MAA, Table S2: Kinetic models of MAA on fluoride removal, Table S3: Thermodynamic parameters on MAA.

Author Contributions: Writing—original draft, Y.G.; data curation, Y.G.; methodology, Y.G.; writing—review and editing, Y.G.; formal analysis, K.Y.; software, K.Y.; investigation, J.F.; project administration, J.W.; supervision, J.W.; resources, W.Q. All authors have read and agreed to the published version of the manuscript.

Funding: This research was no external funding.

Institutional Review Board Statement: This research was not involving humans or animals.

Informed Consent Statement: This research was not involving humans.

Data Availability Statement: This research did not report any data.

Acknowledgments: The authors thank Zhenguo Qi for the experimental assistance.

Conflicts of Interest: The authors declare no conflict of interest.

References

1. Lacson, C.F.Z.; Lu, M.-C.; Huang, Y.-H. Fluoride-containing water: A global perspective and a pursuit to sustainable water defluoridation management—An overview. *J. Clean. Prod.* **2020,** *280*, 124236. https://doi.org/10.1016/j.jclepro.2020.124236.
2. Sternitzke, V.; Kaegi, R.; Audinot, J.-N.; Lewin, E.; Hering, J.G.; Johnson, C.A. Uptake of Fluoride from Aqueous Solution on Nano-Sized Hydroxyapatite: Examination of a Fluoridated Surface Layer. *Environ. Sci. Technol.* **2012**, *46*, 802. https://doi.org/10.1021/es202750t.
3. Nagaraj, A.; Pillay, K.; Kumar, S.K.; Rajan, M. Dicarboxylic acid cross-linked metal ion decorated bentonite clay and chitosan for fluoride removal studies. *RSC Adv.* **2020**, *10*, 16791–16803. https://doi.org/10.1039/D0RA00598C.
4. Turner, B.D.; Binning, P.; Stipp, S.L.S. Fluoride removal by calcite: Evidence for fluorite precipitation and surface adsorption. *Environ. Sci. Technol.* **2005**, *39*, 9561–9568. https://doi.org/10.1021/es0505090.
5. Yadav, K.K.; Kumar, S.; Pham, Q.B.; Gupta, N.; Rezania, S.; Kamyab, H.; Yadav, S.; Vymazal, J.; Kumar, V.; Tri, D.Q.; et al. Fluoride contamination, health problems and remediation methods in Asian groundwater: A comprehensive review. *Ecotoxicol. Environ. Saf.* **2019**, *182*, 109362. https://doi.org/10.1016/j.ecoenv.2019.06.045.
6. Chen, X.; Wan, C.; Yu, R.; Meng, L.; Wang, D.; Chen, W.; Duan, T.; Li, L. A Novel Carboxylated Polyacrylonitrile Nanofibrous Membrane with High Adsorption Capacity for Fluoride Removal from Water. *J. Hazard. Mater.* **2021**, *411*, 125113. https://doi.org/10.1016/j.jhazmat.2021.125113.
7. Bo, Z.; Mei, H.; Yongsheng, Z.; Xueyu, L.; Xuelin, Z.; Jun, D. Distribution and Risk Assessment of Fluoride in Drinking Water in the West Plain Region of Jilin Province, China. *Environ. Geochem. Health* **2003**, *25*, 421–*431*. https://doi.org/10.1023/B:EGAH.0000004560.47697.91.
8. Luo, W.; Gao, X.; Zhang, X. Geochemical processes controlling the groundwater chemistry and fluoride contamination in the yuncheng basin, Chinadan area with complex hydrogeochemical conditions. *PLoS ONE* ***2018***, *13*, e0199082. https://doi.org/10.1371/journal.pone.0199082.
9. Viswanathan, N.; Meenakshi, S. Role of metal ion incorporation in ion exchange resin on the selectivity of fluoride. *J. Hazard. Mater.* **2009**, *162*, 920–930. https://doi.org/10.1016/j. jhazmat.2008.05.118.

10. Li, Q.; Wang, B.; Li, W.; Wang, C.; Zhou, Q.; Shuang, C.; Li, A. Performance evaluation of magnetic anion exchange resin removing fluoride. *J. Chem. Technol. Biotechnol.* **2016**, *91*, 1747–1754. https://doi.org/10.1002/jctb.47641.
11. Arahman, N.; Mulyati, S.; Lubis, M.R.; Takagi, R.; Matsuyama, H. The removal of fluoride from water based on applied current and membrane types in electrodialyis. *J. Fluor. Chem.* **2016**, *191*, 97–102. https://doi.org/10.1016/j.jfluchem.2016.10.002.
12. Boubakri, A.; Bouchrit, R.; Hafiane, A.; Bouguecha, S.A. Fluoride removal from aqueous solution by direct contact membrane distillation: Theoretical and experimental studies. *Environ. Sci. Pollut. Res.* **2014**, *21*, 10493–10501. https://doi.org/10.1007/s11356-014-2858-z.
13. Dhawane, S.H.; Khan, A.A.; Singh, K.; Tripathi, A.; Hasda, R.; Halder, G. Insight into Optimization, isotherm, kinetics, and thermodynamics of fluoride adsorption onto activated alumina. *Environ. Prog. Sustain.* **2018**, *37*, 766–776. https://doi.org/10.1002/ep.12814.
14. Kumari, U.; Behera, S.K.; Meikap, B.C. A novel acid modified alumina adsorbent with enhanced defluoridation property: Kinetics, isotherm study and applicability on industrial wastewater. *J. Hazard. Mater.* **2019**, *365*, 868–882. https://doi.org/10.1016/J.JHAZMAT.2018.11.064.
15. Li, L.; Zhao, L.; Ma, J.; Tian, Y. Preparation of graphene oxide/chitosan complex and its adsorption properties for heavy metal ions. *Green Process. Synth.* **2020**, *9*, 294–303. https://doi.org/10.1515/gps-2020-0030.
16. Tripathy, S.S.; Bersillon, J.L.; Gopal, K. Removal of fluoride from drinking water by adsorption onto alum-impregnated activated alumina. *Sep. Purif. Technol.* **2006**, *50*, 310–317. https://doi.org/10. 1016/j. seppur.2005.11.036.
17. Tripathy, S.S.; Raichur, A.M. Abatement of fluoride from water using manganese dioxide-coated activated alumina. *J. Hazard. Mater.* **2008**, *153*, 1043–1051. https://doi.org/10.1016/j.jhazmat.2007.09.100.
18. Maliyekkal, S.M.; Shukla, S.; Philip, L.; Nambi, M. Enhanced fluoride removal from drinking water by magnesia-amended activated alumina granules. *Chem. Eng. J.* **2008**, *140*, 183–192. https://doi.org/10.1016/j.cej.2007.09.049.
19. Cheng, J.; Meng, X.; Jing, C.; Hao, J. La^{3+}-modified activated alumina for fluoride removal from water. *J. Hazard. Mater.* **2014**, *278*, 343–349. https://doi.org/10.1016/j.jhazmat.2014.06.008.
20. Lenoble, V.; Laclautre, C.; Serpaud, B.; Deluchat, V.; Bollinger, J.-C. As(V) retention and As(III) simultaneous oxidation and removal on a MnO_2-loaded polystyrene resin. *Sci. Total. Environ.* **2004**, *326*, 197–207. https://doi.org/10.1016/j.scitotenv.2003.12.012.
21. Bayoudh, A.; Etteyeb, N.; Kossai, R. Hydrothermal synthesis, characterization and electrochemical properties of γ-MnOOH nanobelts. *Ceram. Int.* **2015**, *41*, 12273–12279. https://doi.org/10.1016/j.ceramint.2015.06.051.
22. Maliyekkal, S.M.; Sharma, A.K.; Philip, L. Manganese-oxide-coated alumina: A promising sorbent for defluoridation of water. *Water Res.* **2006**, *40*, 3497–3506. https://doi.org/10.1016/j.watres.2006.08.007.
23. Guo, X.; Wang, J. Sorption of antibiotics onto aged microplastics in freshwater and seawater. *Mar. Pollut. Bull.* **2019**, *149*, 110511. https://doi.org/10.1016/j.marpolbul.2019.110511.
24. Jwa, B.; Xuan, G.A. Adsorption kinetic models: Physical meanings, applications, and solving methods. *J. Hazard. Mater.* **2020**, *390*, 122156. https://doi.org/10.1016/j.jhazmat.2020.122156.
25. Hu, Y.; Guo, X.; Chen, C.; Wang, J. Algal sorbent derived from Sargassum horneri for adsorption of cesium and strontium ions: Equilibrium, kinetics, and mass transfer. *Appl. Microbiol. Biotechnol.* **2019**, *103*, 2833–2843. https://doi.org/10.1007/s00253-019-09619-z.
26. Ahmed, M.J.; Theydan, S.K. Microwave assisted preparation of microporous activated carbon from Siris seed pods for adsorption of metronidazole antibiotic. *Chem. Eng. J.* **2013**, *214*, 310–318. https://doi.org/10.1016/j.cej.2012.10.101.
27. Boyd, G.E.; Schubert, J.; Adamson, A.W. The exchange adsorption of ions from aqueous solutions by organic zeolites; Kinetics, *J. Am. Chem. Soc.* **1947**, *69*, 2818. https://doi.org/10.1021/ja01203a062.
28. Liu, Y.; Shen, L. From Langmuir kinetics to first- and second-order rate equations for adsorption. *Langmuir* **2008**, *24*, 11625–11630. https://doi.org/10.1021/la801839b.
29. Varghese, S.P.; Babu, A.T.; Babu, B.; Antony, R. γ-MnOOH nanorods: Efficient adsorbent for removal of methylene blue from aqueous solutions. *J. Water Process. Eng.* **2017**, *19*, 1–7. https://doi.org/10.1016/j.jwpe.2017.06.001.
30. Shen, X.; Yan, F.; Li, C.; Qu, F.; Wang, Y.; Zhang, Z. Biogas Upgrading via Cyclic CO_2 Adsorption: Application of Highly Regenerable PEI@nano-Al_2O_3 Adsorbents with Anti-Urea Properties. *Environ. Sci. Technol.* **2021**, *55*, 5236–5247. https://doi.org/10.1021/acs.est.0c07973.
31. Bochatay, L.; Persson, P.; Sjöberg, S. Metal ion coordination at the water-manganite (gamma-MnOOH) interface II. An EXAFS study of zinc(II). *J. Colloid Interface Sci.* **2000**, *229*, 584–592. https://doi.org/10.1006/jcis.2000.7013.
32. Pan, B.; Xu, J.; Wu, B.; Li, Z.; Liu, X. Enhanced Removal of Fluoride by Polystyrene Anion Exchanger Supported Hydrous Zirconium Oxide Nanoparticles. *Environ. Sci. Technol.* **2013**, *47*, 9347–9354. https://doi.org/10.1021/es401710q.
33. Mahmoud, A.E.D.; Hosny, M.; El-Maghrabi, N.; Fawzy, M. Facile synthesis of reduced graphene oxide by Tecoma stans extracts for efficient removal of Ni (II) from water: Batch experiments and response surface methodology. *Sustain. Environ. Res.* **2022**, 32(1). https://doi.org/10.1186/s42834-022-00131-0.
34. Mahmoud, A.E.D.; Al-Qahtani, K.M.; Alflaij, S.O.; Al-Qahtani, S.F.; Alsamhan, F.A. Green copper oxide nanoparticles for lead, nickel, and cadmium removal from contaminated water. *Sci. Rep.* **2021**, *11*, 12547. https://doi.org/10.1038/s41598-021-91093-7.
35. You, K.; Li, P.; Fu, J.; Kang, N.; Gao, Y.; Cheng, X.; Yang, Y.; Yu, F. Fabrication of Manganese-Supported Activated Alumina Adsorbent for Defluoridation of Water: A Kinetics and Thermodynamics Study. *Water* **2021**, *13*, 1219. https://doi.org/10.3390/w13091219.

36. Rayalu, D.S. Synthesis and characterization of lanthanum impregnated chitosan flakes for fluoride removal in water. *Desalination* **2011**, *273*, 267–275. https://doi.org/10.1016/j.desal.2010.12.032.
37. Dhanasekaran, P.; Sahu, O. Arsenate and fluoride removal from groundwater by sawdust impregnated ferric hydroxide and activated alumina (SFAA). *Groundw. Sustain. Dev.* **2021**, *12*, 100490. https://doi.org/10.1016/j.gsd.2020.100490.